Light-Activated Gigahertz Ferroelectric Domain Dynamics

Hirofumi Akamatsu, Yakun Yuan, Vladimir A. Stoica, Greg Stone, Tiannan Yang, Zijian Hong, Shiming Lei, Yi Zhu, Ryan C. Haislmaier, John W. Freeland, Long-Qing Chen, Haidan Wen, and Venkatraman Gopalan

Phys. Rev. Lett. **120**, 096101 — Published 26 February 2018

DOI: 10.1103/PhysRevLett.120.096101

Light-activated Gigahertz Ferroelectric Domain Dynamics

Hirofumi Akamatsu,[1] Yakun Yuan,[1] Vladimir Stoica,[1,2] Greg Stone,[1] Tiannan Yang,[1] Zijian Hong,[1] Shiming Lei,[1] Yi Zhu,[2] Ryan C. Haislmaier,[1] John W. Freeland,[2] Long-Qing Chen,[1] Haidan Wen,[2] and Venkatraman Gopalan[1,*]

[1]*Materials Research Institute and Department of Materials Science and Engineering, Pennsylvania State University, MSC Building, University Park, Pennsylvania 16802, USA*
[2]*Advanced Photon Source, Argonne National Laboratory, Argonne, Illinois 60439, USA*

(Dated: January 5, 2018)

Using time- and spatially-resolved hard X-ray diffraction microscopy, the striking structural and electrical dynamics upon optical excitation of a single crystal of $BaTiO_3$ are simultaneously captured on sub-nanoseconds and nanoscale within individual ferroelectric domains and across walls. A large emergent photo-induced electric field of up to 20 million volts per meter is discovered in a surface layer of the crystal, which then drives polarization and lattice dynamics that are dramatically distinct in a surface layer versus bulk regions. A dynamical phase-field modeling (DPFM) method is developed that reveals the microscopic origin of these dynamics, leading to GHz polarization and elastic waves travelling in the crystal with sonic speeds and spatially varying frequencies. The advance of spatiotemporal imaging and dynamical modeling tools open opportunities of disentangling ultrafast processes in complex mesoscale structures such as ferroelectric domains

The fast-paced improvements in ultrafast radiation from X-ray and ultraviolet to terahertz (THz) frequencies is enabling simultaneous probe of electron, phonon, and spin dynamics on ps-to-ns time scales, as well as sub-micrometer length scales [1–10]. There is emerging recognition now that ultrafast dynamics and the appearance of new phenomena depend not only on the intrinsic properties of the compound, but also strongly depend on the mesoscale structure such as surfaces, domains, walls, interfaces and defects that govern the coupling between various order parameters [11]. Previous experimental studies on the dynamics of ferroelectrics largely fall into two categories: high spatial resolution (down to nanometer or atomic scale) but slow temporal resolution (ms and above) [12–20], or high temporal resolution (down to 100 fs), but low spatial resolution (10's of microns and above) [21–24]. Although the latter provides structural information on the atomistic scales by ultrafast X-ray diffraction, the mesoscale dynamics of domain evolution is spatially averaged [10, 24–27]. A key challenge in disentangling these results is that the former is not suited to discover transient phenomena on ultrafast time scales, while in the latter case, the intricate details of the local dynamics can be lost via spatially averaged probes.

Here, we report on simultaneous high-resolution spatial and temporal mapping of domains and domain walls in a multi-domain ferroelectric bulk single crystal of $BaTiO_3$ using ultrafast X-ray and optical pulses. Analysis of the spatio-temporal structural dynamics reveals an emergent electric field around 20 MV/m is induced by irradiating the surface with 400 nm fs optical pulses, resulting in GHz polarization and lattice waves. Stroboscopic probing by X-ray pulses that are ≈100 ps in duration and ≈350 nm in size [28], yields atomistic structural dynamics within individual domains and across domain walls. Low frequency GHz acoustic pulses excited within domains are spatially tracked in different domain orientations and across domain walls. A dynamical phase-field modeling (DPFM) method is developed to show that this large surface field tilts the polarization of the *a*-domain out-of-plane, and sets up a GHz wave which expands the *c*-domains and shrinks the *a*-domains in a damped oscillatory motion on pico-to-nanosecond time scales [24]. Excellent agreement is observed between the modeling and the experiments. The combination of theory and experiments reveals subsonic domain wall motion at speeds of 2.5 m/s within in the first nanosecond after optical excitation, approaching the ultimate speed limit of wall motion of a few unit cells on sub-nanosecond time scales [29]. The spatial dependence of the surface and subsurface domain dynamics uncovered by this work highlights the value of such spatiotemporal studies combined with dynamical phase field modeling in understanding ultrafast phenomena in complex mesoscale domain structures.

The $BaTiO_3$ single crystal is one of the earliest ferroelectrics discovered [30–32]. At room temperature, it exhibits a tetragonal structure with a point group symmetry of $4mm$. The crystal used in this study contains both *a*-domains, with polarization parallel to the crystal surface (depicted in green); and *c*-domains, with polarization normal to the crystal surface (depicted in yellow) as illustrated in Fig. 1(a). The *a*-domains and *c*-domains are separated by 90° domain walls and are clearly revealed by piezoresponse force microscopy image of the crystal surface [Fig. 1(b)]. Along the depth of the crystal, the domain walls are aligned at 45° with respect to the crystal surface. The acquisition of spatio-temporal X-ray diffraction (XRD) maps of these domains was performed on the 7ID-C beamline at the Advanced Photon Source at the Argonne National Laboratory, and is depicted in Fig. 1(a) (see details in Supplemental section I [33]). Figure 1(c) schematically depicts the *a*- and *c*-domain depth profile, and their respective lattice spac-

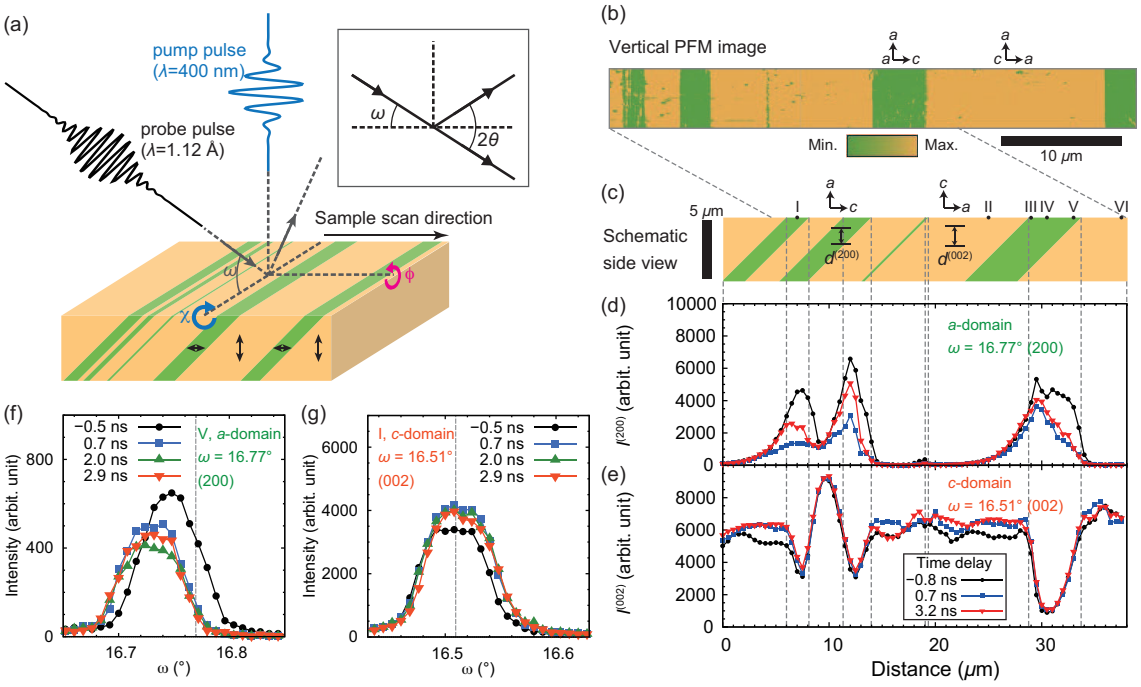

FIG. 1: (Color online) (a) Schematic illustration of spatially-resolved pump-probe experiment and domain configuration of $BaTiO_3$ single crystal sample. The inset illustrates the incident plane. The tilting angles of domains, χ and ϕ, are also shown. a- and c-domains are depicted in green and orange colors, respectively. (b) Vertical piezoresponse force microscopy image on the top surface. (c) Schematic domain wall structures derived from spatial mapping of (200) and (002) reflection intensities at ω=16.77° and 16.51° for various time delays shown in (d) and (e), respectively. The ω scan profiles for various time delays around (f) (200) and (g) (002) reflections at the location V and I, respectively, labeled in panel (c).

ing $d^{(200)}$ and $d^{(002)}$, within the crystal, and the corresponding X-ray probe locations (marked as I through VI). In the area of interest, a fractional volume of a-domains is ≈30%. An optical pump pulse with 400 nm in wavelength was derived by doubling the output of an Ti:Sapphire laser, and passed through a fused silica rod to lengthening the pulse duration for avoiding sample surface damage. This pump laser pulse with a pulse duration of 330-560 fs then was focused to 50 μm diameter on the sample with a penetration depth of 30 μm. Given the penetration depth of X-ray pulses with a photon energy of 11 keV (≈10 μm) [Figure S1(c) of the Supplemental section Ⅱ [33]], XRD intensity was observed from both the surface and the underlying subsurface domains at many locations across the sample, shown as well-separated diffraction peaks recorded on the area detector. The surface and subsurface domain type, a or c, can be determine from the corresponding XRD intensity from each domain [Figs. 1(d) and (e)]. Observed changes in the XRD intensity arise from both crystal distortions and rotations. To separate the two effects, rocking curves at different probe delay times were collected in Figs. 1(f) and (g). Both the line scans at different pump-probe time delays [Figs. 1(d) and (e)] along with the rocking curves [Figs. 1(f) and (g)] form a complete spatiotemporal data set for this crystal.

We focus our attention on six spatial locations (I-VI) across different domain walls for the analyses of the spatiotemporal X-ray data; these locations are indicated in Fig. 2(a), and the relevant d-spacing are indicated in the schematic diagram of Fig. 2(b). Of these, locations labeled I, Ⅲ, IV, and V are surface a-domains, and locations Ⅱ and VI are surface c-domains. For each of the four above-listed a-domain locations, there is a subsurface c-domain underneath it, and similarly for both c-domain imaged locations, there is a subsurface a-domain. Figure 2(c) plots the temporal diffraction intensity changes at fixed diffraction angle for the surface a-domain as well as subsurface c-domain at position I. Clear oscillations are observed with nanosecond periodicities that indicate GHz frequencies. By performing the ω-2θ scans at each time delay for a number of spatial locations, one can extract the changes in the out-of-plane lattice parameter $\Delta d/d_0^{(200)}$ and $\Delta d/d_0^{(002)}$, as plotted in Figs. 2(d) and (e). The green curves are the surface a-domains at location I and subsurface a-domains at location Ⅱ. The orange curves are the subsurface c-domains at location I and surface c-domains at location Ⅱ. Similar data was collected for spatial locations Ⅲ-VI (see Fig. S2 of the Supplemental section Ⅲ [33]).

We first make some general observations from the spatio-temporal domain dynamics: There are two dis-

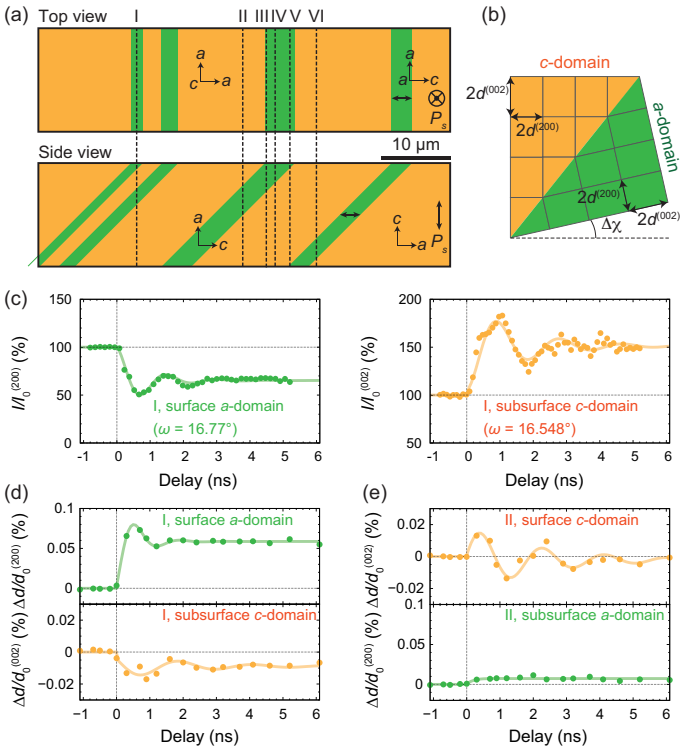

FIG. 2: (Color online) (a) Locations I to VI at which time-delay dependent XRD measurements were performed. (b) Lattice spacings of (200) and (002) planes for a- and c-domains are illustrated. The difference between rotation angles χ's for a- and c-domains, $\Delta\chi$, is depicted. (c) Time-delay dependence of (200) (ω=16.77°) and (002) (ω=16.548°) intensities relative to those before t=0, $I/I_0^{(200)}$ and $I/I_0^{(002)}$, respectively, at the location I taken with pump fluence of 66.2 mJ/cm^2. The (200) and (002) lattice-spacing change for a- and c-domains from those before t=0, $\Delta d/d_0^{(200)}$ and $\Delta d/d_0^{(002)}$, respectively, as a function of time delay at the locations (d) I (left) and (e) II (right). Solid lines in (c)-(e) are fits by a damped oscillator model.

tinct sets of structural dynamics, i.e., surface and subsurface. We estimate the upper bound for the surface region to be confined to a depth of ≤700 nm, as indicated by the data taken at the location V, where the subsurface c-domain buried ≈700 nm underneath exhibits lattice dynamics behavior characteristic of the subsurface region (see Fig. S2 of the Supplemental section Ⅲ [33]). After photoexcitation, the out-of-plane lattice spacing increases within the first ≈100-150 ps for both the surface a-domain ($\Delta d/d_0^{(200)}$≈0.06-0.08%), and the surface c-domains ($\Delta d/d_0^{(002)}$≈0.02%). In contrast, the out-of-plane lattice spacing slightly increases for the subsurface a-domain ($\Delta d/d_0^{(200)}$≈0.01%), and decreases for the subsurface c-domain ($\Delta d/d_0^{(002)}$≈−0.02%) within the same time period. Thereafter, oscillations about this new lattice spacing with a damping time constant of a few nanoseconds are observed, which decay back to zero (not shown) by the time the subsequent optical pulse arrives at the sample (∼1 ms).

To quantitatively understand the dynamics, we fit the time-dependent $\Delta d/d_0^{(200)}$ and $\Delta d/d_0^{(002)}$ data, Figs. 2(d) and (e), after time zero using the following damped acoustic oscillator model: $\Delta d/d_0(t) = A + B\exp(-\gamma t)\cos[2\pi\nu(t-\phi)]$. The fitting parameters at all the locations are given in the Tables S1 and S2 of the Supplemental section Ⅳ [33]. Typically, the oscillation frequency falls between ν≈0.2-0.7 GHz with a damping rate of γ≈0.03-5 ns^{-1}. The 90° domain walls intersect the surface at 45° and create wedge-like surface domains viewed from the cross-section. By plotting twice the domain thickness l of the wedge-shaped surface a- and c-domains, versus the ν^{-1} of the GHz waves at that location on the wedge (See Fig. S4 of the Supplemental section Ⅳ [33]), we observe an approximate linear trend of increasing inverse oscillation frequency ν^{-1} with increasing wedge thickness l. The slope $2l/\nu^{-1}$≈5.9×10^3 m/s, obtained from Figure S4 is strikingly close to the reported speed of sound in $BaTiO_3$ of ≈5.2×10^3 m/s [34]. This suggests that vertical oscillations of the surface reflect standing elastic waves of sonic frequency between the surface and the subsurface domain walls. Through DPFM, we will demonstrate shortly that these oscillations arise from polarization dynamics.

We focus next on the differences in structural dynamics between surface and subsurface regions, and their underlying mechanism. One notes from Figs. 2(d) and (e), that the c-lattice parameter initially increases for surface c-domains [see Fig. 2(e), location Ⅱ], which at first glance seems contrary to a pure thermal effect [35]. We also carefully considered whether such a lattice parameter change could arise due to local optical heating of a region that is clamped by the surrounding unheated region; using dynamical phase-field modeling (DPFM) as described further on, we cleanly rule out this possibility (See the Supplemental section Ⅶ [33]). Further, the maximum expected temperature change, ΔT, due to the linear absorption of optical pump is small, <0.5°C (See Fig. S1(d) of the Supplemental section Ⅱ [33]). By estimating the nonlinear absorption from Ref. 36, the overall temperature change expected for our experimental pump fluence of 66.2 mJ/cm^2 is ΔT∼1-10°C; a nonlinear coefficient of 2.3 cm/GW gives rise to a temperature change of ∼6°, which gives the best DPFM fit to experiments as described next. Lattice parameter changes caused only by thermal expansion are a half order of magnitude smaller than the changes in the surface lattice parameters observed experimentally. Finally, the pump-fluence dependence of domain dynamics shown in the Supplemental section Ⅴ [33] clearly indicates that the time constant decreases at higher pump fluences. Since the time constant for thermal diffusion should be independent of the temperature change and hence the pump fluence, this suggests that the observed structural changes are not purely

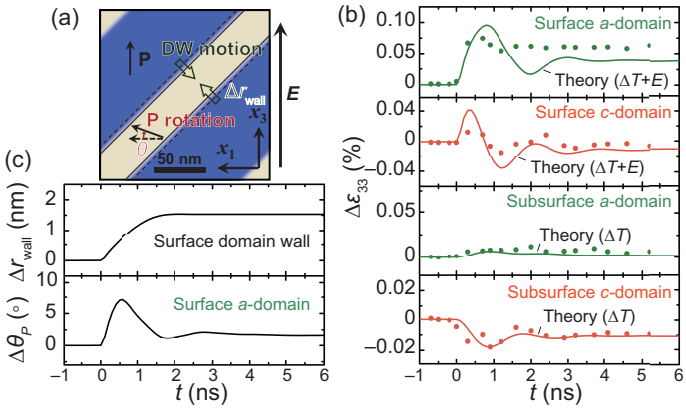

FIG. 3: (Color online) (a) The a- and c-domain configuration used in the DPFM. The displacement of the 90° domain walls ($\Delta r_{\rm wall}$) and a rotation of the polarization inside a domain towards the out-of-plane direction ($\Delta\theta$) are illustrated as the effect of the field in the surface layer. (b) The experimental and theoretical $\Delta\epsilon_{33}$ as a function of time, in the surface and subsurface domains. (c) $\Delta r_{\rm wall}$ and $\Delta\theta$ as a function of time in the crystal surface layer under the photo-induced electric field.

driven by thermal diffusion. Because of all these reasons, we need to consider additional non-thermal effects.

To understand the complex dynamics on ultrafast time scale revealed by experiments above, we have developed a DPFM approach. The dynamic response of the polarization $\mathbf{P}(\mathbf{r})$ is described using the modified time-dependent Ginzburg-Landau equation with an additional term in the second-derivative of $\mathbf{P}$ with respect to time, accounting for intrinsic oscillation of the polarization, written as

$$\mu\frac{\delta^2\mathbf{P}}{\delta t^2}+\gamma\frac{\delta\mathbf{P}}{\delta t}+\frac{\delta F}{\delta\mathbf{P}}=0, \qquad (1)$$

where μ and γ are kinetic coefficients related to domain wall mobility. The equation is numerically solved using a semi-implicit Fourier spectral method. $F=F_{Landau}+F_{gradient}+F_{electric}+F_{elastic}$ is the total free energy of the ferroelectric $BaTiO_3$, where F_{Landau}, $F_{gradient}$, $F_{electric}$, and $F_{elastic}$ are the ferroelectric landau free energy, ferroelectric gradient energy, electrostatic energy, and elastic energy, respectively, with formulations given in Refs.[37, 38]. The details of the DPFM modeling are described in the Supplemental section VI [33].

DPFM was performed for a $BaTiO_3$ crystal with periodic boundary conditions as shown in Fig. 3(a). A pure temperature change of $\Delta T\sim6$°C results in excellent agreement with the experimentally observed lattice distortions in the subsurface region indicated in Fig. 3(b). However, a pure thermal effect is insufficient to explain the experimentally observed surface structural dynamics within the $\leq$700 nm depth near the surface. Motivated by past reports of a possible surface layer [39–45], we explored an electric field of $\approx2\times10^7$ V/m in the DPFM, parallel to the polarization direction in the c-domains, and perpendicular to the polarization direction in the a-domains. When this field is combined with a temperature change of $\Delta T\approx6$°C, the DPFM predicts the GHz oscillations that are in outstanding agreement with experiments, as seen in Fig. 3(b), and thus provides insight into their origin. The impulsive photo-induced electric field of 20 MV/m expands c-domains and shrinks the a-domains by activating domain wall motions. As a result, the c-domain grows by $\approx$4 unit cells or $\approx$1.5 nm within 0.6 ns, leading to a subsonic domain growth speed of 2.5 m/s within the first nanosecond after excitation [Fig. 3(c)]. In addition, the photo-induced surface field induces a polarization normal to the surface and tilts the polarization of the a-domain from in-plane to the out-of-plane direction by up to 7.5° over 0.5 ns, which leads to an increase in the out-of-plane lattice spacing [Fig. 3(c)]. The slight expansion of the c-domains, and the tilting of the polarization in a-domains leads to polarization and lattice waves that propagate at the speed of sound and exhibit a damped oscillatory behavior with GHz frequencies. The outstanding agreement between experiments and DPFM, for both surface and subsurface lattice behavior, each for both a- and c-domains [Fig. 3(a)] enables these insights. Surface layer electric field geometries in DPFM other than the out-of-plane field discussed above gave poor agreement with the experiments (see Fig. S8 of the Supplemental section VIII [33]), thus ruling them out. The slight dynamic expansion of the c-domain was confirmed using optical pump, optical second harmonic generation (SHG) probing [See the Supplemental section IX [33]]. Our SHG polarimetry shows a c-domain fraction of $\approx$54.8% before 400 nm optical pumping and $\approx$57.7%, 2 ns after pumping.

In conclusion, spatio-temporal imaging of the structural and polarization dynamics of ferroelectric domains using ultrafast XRD microscopy, combined with a newly developed DPFM code reveals a large emergent photo-induced surface layer electric field of 20 MV/m in the surface region ($\leq$700 nm) of $BaTiO_3$ single crystals that is created by an optical pump pulse. This temporal electric field sets up polarization dynamics that involves impulsively tilting the polarization of a-domains out of the plane of the crystal and expanding the c-domains at subsonic speeds, that lead to GHz polarization and elastic waves that are directly imaged. The excellent agreement between DPFM and experiments help reveal many of the subtleties of the emergent ultrafast phenomena observed in this study. In contrast to spatially averaged ultrafast studies, spatio-temporally resolved experiments such as this study and others under development [3, 6, 14, 46], combined with new theory tools such as DPFM will become increasingly critical towards a fundamental understanding of ultrafast emergent phenomena on the mesoscale.

H.A., Y.Y., V.S., H.W., J.F. and V.G. were supported

by the U.S Department of Energy, Office of Science, Office of Basic Energy Sciences, under grant No. DE-SC0012375, for the ultrafast XRD microscopy and ultrafast optical pump SHG probe work. The use of Advanced Photon Source was supported by the U.S Department of Energy, Office of Science, Office of Basic Energy Sciences, under Contract No. DE-AC02-06CH11357. G.S., S.L., R.H., and Z.H. were supported by NSF grant NO. DMR-1420620 for the XRD data analysis, PFM measurements, UV-vis absorption measurements, and DPFM. T.Y. and L.Q.C. acknowledge the support by NSF under grant No. DMR-1410714 for the DPFM work. We would like to thank Prof. Aaron Lindenberg, Burak Guzelturk, Dr. Jianjun Wang, Dr. Fei Xue for helpful discussions and suggestions on the DPFM.

* e-mail:vxg8@psu.edu

[1] J. Zhang and R. Averitt, Annu. Rev. Mater. Res. **44**, 19 (2014).

[2] F. Chen, J. Goodfellow, S. Liu, I. Grinberg, M. C. Hoffmann, A. R. Damodaran, Y. Zhu, P. Zalden, X. Zhang, I. Takeuchi, et al., Advanced Materials **27**, 6371 (2015).

[3] E. Szilagyi, J. S. Wittenberg, T. A. Miller, K. Lutker, F. Quirin, H. Lemke, D. Zhu, M. Chollet, J. Robinson, H. Wen, et al., Nat. Commun. **6**, 6577 (2015).

[4] W. Hu, S. Kaiser, D. Nicoletti, C. R. Hunt, I. Gierz, M. C. Hoffmann, M. Le Tacon, T. Loew, B. Keimer, and A. Cavalleri, Nat. Mater. **13**, 705 (2014).

[5] B. Zhang, D. F. Gardner, M. D. Seaberg, E. R. Shanblatt, H. C. Kapteyn, M. M. Murnane, and D. E. Adams, Ultramicroscopy **158**, 98 (2015).

[6] M. D. Seaberg, B. Zhang, D. F. Gardner, E. R. Shanblatt, M. M. Murnane, H. C. Kapteyn, and D. E. Adams, Optica **1**, 39 (2014).

[7] M. Matsubara, A. Schroer, A. Schmehl, A. Melville, C. Becher, M. Trujillo-Martinez, D. G. Schlom, J. Mannhart, J. Kroha, and M. Fiebig, Nat. Commun. **6** (2015).

[8] H. Wen, L. Guo, E. Barnes, J. H. Lee, D. A. Walko, R. D. Schaller, J. A. Moyer, R. Misra, Y. Li, E. M. Dufresne, et al., Phys. Rev. B **88**, 165424 (2013).

[9] H. Wen, P. Chen, M. P. Cosgriff, D. A. Walko, J. H. Lee, C. Adamo, R. D. Schaller, J. F. Ihlefeld, E. M. Dufresne, D. G. Schlom, et al., Phys. Rev. Lett. **110**, 037601 (2013).

[10] D. Daranciang, M. J. Highland, H. Wen, S. M. Young, N. C. Brandt, H. Y. Hwang, M. Vattilana, M. Nicoul, F. Quirin, J. Goodfellow, et al., Phys. Rev. Lett. **108**, 087601 (2012).

[11] M. Liu, A. J. Sternbach, and D. N. Basov, Rep. Prog. Phys. **80**, 014501 (2017).

[12] M. Matsubara, S. Manz, M. Mochizuki, T. Kubacka, A. Iyama, N. Aliouane, T. Kimura, S. L. Johnson, D. Meier, and M. Fiebig, Science **348**, 1112 (2015).

[13] C. T. Nelson, P. Gao, J. R. Jokisaari, C. Heikes, C. Adamo, A. Melville, S.-H. Baek, C. M. Folkman, B. Winchester, Y. Gu, et al., Science **334**, 968 (2011).

[14] S. O. Hruszkewycz, M. J. Highland, M. V. Holt, D. Kim, C. M. Folkman, C. Thompson, A. Tripathi, G. B. Stephenson, S. Hong, and P. H. Fuoss, Phys. Rev. Lett. **110**, 177601 (2013).

[15] P. Gao, J. Britson, C. T. Nelson, J. R. Jokisaari, C. Duan, M. Trassin, S.-H. Baek, H. Guo, L. Li, Y. Wang, et al., Nat. Commun. **5** (2014).

[16] T. T. A. Lummen, Y. Gu, J. Wang, S. Lei, F. Xue, A. Kumar, A. T. Barnes, E. Barnes, S. Denev, A. Belianinov, et al., Nat. Commun. **5** (2014).

[17] A. Grigoriev, R. J. Sichel, J. Y. Jo, S. Choudhury, L.-Q. Chen, H. N. Lee, E. C. Landahl, B. W. Adams, E. M. Dufresne, and P. G. Evans, Phys. Rev. B **80**, 014110 (2009).

[18] P. Chen, M. P. Cosgriff, Q. Zhang, S. J. Callori, B. W. Adams, E. M. Dufresne, M. Dawber, and P. G. Evans, Phys. Rev. Lett. **110**, 047601 (2013).

[19] F.-T. Huang and S.-W. Cheong, Nat. Rev. **2**, 17004 (2017).

[20] X. Wu, U. Petralanda, L. Zheng, Y. Ren, R. Hu, S.-W. Cheong, S. Artyukhin, and K. Lai, Science Adv. **3** (2017).

[21] D. Issenmann, S. Schleef, S. Ibrahimkutty, G. Buth, T. Baumbach, A. Plech, M. Beyer, and J. Demsar, Acta Phys. Pol., A **121**, 319 (2012).

[22] K. Istomin, V. Kotaidis, A. Plech, and Q. Kong, Appl. Phys. Lett. **90**, 022905 (2007).

[23] Y.-H. Kuo, S. Nah, K. He, T. Hu, and A. M. Lindenberg, J. Mater. Chem. C **5**, 1522 (2017).

[24] F. Chen, Y. Zhu, S. Liu, Y. Qi, H. Y. Hwang, N. C. Brandt, J. Lu, F. Quirin, H. Enquist, P. Zalden, et al., Phys. Rev. B **94**, 180104 (2016).

[25] J. Y. Jo, P. Chen, R. J. Sichel, S. J. Callori, J. Sinsheimer, E. M. Dufresne, M. Dawber, and P. G. Evans, Phys. Rev. Lett. **107**, 055501 (2011).

[26] A. Grigoriev, D.-H. Do, D. M. Kim, C.-B. Eom, B. Adams, E. M. Dufresne, and P. G. Evans, Phys. Rev. Lett. **96**, 187601 (2006).

[27] A. Grigoriev, D.-H. Do, D. M. Kim, C.-B. Eom, P. G. Evans, B. W. Adams, and E. M. Dufresne, Int. Ferroelec. **85**, 165 (2006).

[28] Y. Zhu, Z. Cai, P. Chen, Q. Zhang, M. J. Highland, I. W. Jung, D. A. Walko, E. M. Dufresne, J. Jeong, M. G. Samant, et al., Sci. Rep. **6**, 21999 EP (2016).

[29] G. Catalan, J. Seidel, R. Ramesh, and J. F. Scott, Rev. Mod. Phys. **84**, 119 (2012).

[30] A. von Hippel, R. G. Breckenridge, F. G. Chesley, and L. Tisza, Ind. Eng. Chem. **38**, 1097 (1946).

[31] B. Wul and M. Goldman, J, C.R. Acad. Sci. URSS **51**, 21 (1946).

[32] G. H. Kwei, A. C. Lawson, S. J. L. Billinge, and S. W. Cheong, The Journal of Physical Chemistry **97**, 2368 (1993).

[33] See Supplementary Material [url] for the information on experimental details, linear and nonlinear absorption, position dependence of ultrafast lattice responses, details of dynamical phase-field modeling, and second harmonic generation experiments, which includes Refs. [47–55].

[34] *Landolt-Börnstein, New Series: Elastic, Piezoelectric, Piezooptic and Electrooptic Constants of Crystals* (Springer US, Berlin, Heidelberg, 1966).

[35] The c-lattice spacing of $BaTiO_3$ decreases with increasing temperature because of tetragonal distortion accompanied by ferroelectric phase transition above room temperature [34].

[36] S. Liu, J. Xu, D. Guzun, G. Salamo, C. Chen, Y. Lin, and M. Xiao, Appl. Phys. B **82**, 443 (2006).

[37] Y. L. Li, S. Y. Hu, Z. K. Liu, and L. Q. Chen, Appl. Phys. Lett. **78**, 3878 (2001).
[38] Y. L. Li, S. Y. Hu, Z. K. Liu, and L. Q. Chen, Appl. Phys. Lett. **81**, 427 (2002).
[39] H. Motegi, J. Phys. Soc. Japan **32**, 202 (1972).
[40] E. Fatuzzo and W. J. Merz, J. Appl. Phys. **32**, 1685 (1961).
[41] R. E. Nettleton, J. Appl. Phys. **38**, 2775 (1967).
[42] W. J. Merz, J. Appl. Phys. **27**, 938 (1956).
[43] W. Känzig, Phys. Rev. **98**, 549 (1955).
[44] A. G. Chynoweth, Phys. Rev. **102**, 705 (1956).
[45] F. Rubio-Marcos, A. Del Campo, P. Marchet, and J. F. Fernández, Nat. Commun. **6**, 6594 EP (2015).
[46] J. Miao, T. Ishikawa, I. K. Robinson, and M. M. Murnane, Science **348**, 530 (2015).
[47] *Advanced photon source website, compute x-ray absorption [http://11bm.xray.aps.anl.gov/absorb/absorb.php].*
[48] T. F. Boggess, J. O. White, and G. C. Valley, J. Opt. Soc. Am. B **7**, 2255 (1990).
[49] R. A. Ganeev, M. Suzuki, M. Baba, M. Ichihara, and H. Kuroda, J. Opt. Soc. Am. B **25**, 325 (2008).
[50] W. F. Zhang, Y. B. Huang, M. S. Zhang, and Z. G. Liu, Appl. Phys. Lett. **76**, 1003 (2000).
[51] Y. L. Li, L. E. Cross, and L. Q. Chen, J. Appl. Phys. **98**, 064101 (2005).
[52] N. Bloembergen and P. S. Pershan, Phys. Rev. **128**, 606 (1962).
[53] G. Rupprecht and R. O. Bell, Phys. Rev. **135**, A748 (1964).
[54] M. Gorev, V. Bondarev, I. Flerov, M. Maglione, A. Simon, P. Sciau, M. Boulos, and S. Guillemet-Fritsch, Journal of Physics: Condensed Matter **21**, 075902 (2009).
[55] T. Yamada, Journal of Applied Physics **43**, 328 (1972).